Mon. Not. R. Astron. Soc. **000**, 000–000 (0000) Printed 28 August 2014 (MN LATEX style file v2.2)

The jet–disc connection in AGN

T. Sbarrato[1,2,3⋆], P. Padovani[1,4], G. Ghisellini[2]
[1]*ESO – European Southern Observatory, Karl–Schwarzschild–Strasse 2, D–85748 Garching bei München, Germany*
[2]*INAF – Osservatorio Astronomico di Brera, Via Bianchi 46, I–23807 Merate, Italy*
[3]*Università dell'Insubria, Dipartimento di Scienza e Alta Tecnologia, Via Valleggio 11, I–22100 Como, Italy*
[4]*Associated to INAF – Osservatorio Astronomico di Roma, via Frascati 33, I–00040 Monteporzio Catone, Italy*

arXiv:1405.4865v2 [astro-ph.HE] 27 Aug 2014

28 August 2014

ABSTRACT
We present our latest results on the connection between accretion rate and relativistic jet power in AGN, by using a large sample which includes mostly blazars, but contains also some radio–galaxies. The jet power can be traced by γ–ray luminosity in the case of blazars, and radio luminosity for both classes. The accretion disc luminosity is instead traced by the broad emission lines. Among blazars, we find a correlation between broad line emission and the γ–ray or radio luminosities, suggesting a direct tight connection between jet power and accretion rate. We confirm that the observational differences between blazar subclasses reflect differences in the accretion regime, but with blazars only we cannot properly access the low–accretion regime. By introducing radio–galaxies, we succeed in observing the fingerprint of the transition between radiatively efficient and inefficient accretion discs in the jetted AGN family. The transition occurs at the standard critical value $L_{\rm d}/L_{\rm Edd} \sim 10^{-2}$ and it appears smooth. Below this value, the ionizing luminosity emitted by the accretion structure drops significantly.

Key words: BL Lacertae objects: general — quasars: general — accretion, accretion discs — radiation mechanisms: non–thermal — gamma-rays: general

1 INTRODUCTION

Blazars are Active Galactic Nuclei (AGN) with a relativistic jet directed towards our line of sight. Because of relativistic beaming, the emission from the jet is highly boosted, and dominates the AGN emission at all wavelengths, from the radio to the γ–ray band. They are very useful to study the relation between accretion structure and relativistic jet in AGN.

Blazars are commonly divided in Flat Spectrum Radio Quasars (FSRQs) and BL Lacertae objects (BL Lacs), depending on the rest frame equivalent width (EW) of their broad emission lines. Specifically, if the EW is smaller than 5Å, the object is classified as a BL Lac, otherwise as a FSRQ (Urry & Padovani 1995). An analogous classification criterion was introduced by Landt et al. (2004), that found possible to discriminate between objects with intrinsically weak or strong narrow emission lines by studying the [OII] and [OIII] EW plane. The EW–based classification, besides being simple to apply, is based on the fact that the EW is a good measure of the line emission dominance over the non–thermal continuum emitted from the jet. In this view, the EW could tell if an object had intrinsically strong (FSRQ) or weak (BL Lac) emission lines. However, jet emission is extremely variable, definitely more than the thermal continuum and the emission lines. Hence the line EW can dramatically vary from one state to another for the same source. A blazar with intrinsically very luminous emission lines can temporarily appear as a BL Lac, with very small EW, if its jet flux happens to be more luminous than usual. On the contrary, during a particularly low state, a BL Lac can show emission lines with EW larger than the 5Å limit (as it happened to BL Lac itself; Vermeulen et al. 1995; Capetti, Raiteri & Buttiglione 2010). Ghisellini et al. 2011 (hereafter G11) already proposed that this classification is not reliable, and moreover does not reflect any intrinsic property or difference within the blazar class, being dependent on the strong continuum variability. These authors introduced a more physical classification, based on the different accretion rates of the two subclasses of blazars, later confirmed in our earlier work (Sbarrato et al. 2012; hereafter TS12): FSRQs have a disc luminosity $\gtrsim 5\times10^{-3}$ of the Eddington one. In those papers, a strong correlation between accretion and jet emissions was found. The unreliability of the EW classification was also deeply investigated by Giommi et al. (2012; 2013), who suggested that blazars should be divided in high– and low–ionization sources, instead of focusing on observed features that are not physically relevant. In other words, G11, TS12 and Giommi et al. (2012; 2013) based their reclassification on the ionizing luminosity, emitted from the accretion disc.

Radio–galaxies are thought to be the parent population of blazars: while blazars are aligned to our line–of–sight, radio–galaxies have their jets oriented at larger viewing angles. This

⋆ Email: tullia.sbarrato@brera.inaf.it

© 0000 RAS

greatly affects the overall emission and the typical Spectral Energy Distribution (SED), that is not dominated by the non–thermal radiation in the case of radio–galaxies, contrary to blazars (Urry & Padovani 1995). Radio–galaxies are historically divided into two subclasses according to their radio morphology (Fanaroff & Riley 1974): FRI show bright jets close to the nucleus, while FRII show prominent hot spots far from it. This classification also reflects in a separation in their radio power (below and above $L_{178\mathrm{MHz}} = 2.5 \times 10^{33}\,\mathrm{erg\,s^{-1}\,Hz^{-1}}$, respectively). As in the case of blazars, the classification is not sharp, but radio–galaxies seem to be distributed continuously between the two classes. Similarly to the blazar case, radio–galaxies were also classified according to their ionization efficiency. In the nineties many spectroscopic–based classifications were proposed, also connecting the emission line luminosities to the radio power (e.g. Baum & Heckman 1989a,b; Rawlings et al. 1989; Rawlings & Saunders 1991; Morganti et al. 1997; Labiano 2008; Willott et al. 1999). Ghisellini & Celotti (2001) showed that the division between FRI and FRII actually reflected a systematic difference in accretion rate: FRI were shown to have generally an ionizing luminosity $\sim 10^{-2} - 10^{-3}$ of the Eddington one, while for FRII this was typically larger. Laing et al. (1994) introduced a sub–classification of FRII sources into high–excitation (HEG) and low–excitation galaxies (LEG), but this was found to be applicable also to some FRI. Therefore, Buttiglione et al. (2009; 2010) decided to perform an extended investigation of the spectroscopic properties of radio–galaxies, using a homogeneous sample. They found that all HEG are FRII, while LEG can be both FRI and FRII. While a ionization–based classification seems to be more physically relevant also in the case of radio–galaxies, an univocal, physically based classification method is not yet commonly accepted, as in the case of blazars.

In this work, we try to investigate the relation between accretion and jet emissions in jetted AGN, to understand if a change in the accretion mode happens inside the blazar family, and the whole jetted AGN class. We enlarge the blazar sample with respect to the one in TS12, and we extend our study to another tracer of the jet power: radio luminosity. In this way, we can also include radio–galaxies to study the jet–accretion relation in the whole family of jetted AGN. Section 2 presents the samples, Section 3 describes how we trace the accretion luminosity through the broad line region emission. In Section 4 we investigate the relationship between broad line region and γ–ray power, while the one between broad line region and radio power is dealt with in Section 5. The discussion is presented in Section 6, and our results are summarized in Section 7.

2 THE SAMPLE

We are interested in studying the relationship between jet and accretion in AGN, through γ–ray or radio luminosity and broad line region (BLR) luminosity, respectively. We first tried to study it among the blazar subclass, by collecting a complete sample of γ–ray detected blazars, with measurements of the luminosity of broad lines obtained through optical spectroscopy. We then extended our sample to radio–galaxies intrinsically without broad emission lines (but with known redshift), to investigate the jet–accretion relationship in the inefficient accretion regime. Even if not complete, the radio–galaxy sample we describe in §2.2 is the most useful for our purposes, as the ionization status of every member is throughly studied.

2.1 The blazar samples

The Large Area Telescope (LAT) onboard the *Fermi Gamma-Ray Space Telescope* (*Fermi*) has detected a large amount of blazars in the γ–rays. In two different papers (Shaw et al. 2012 and Shaw et al. 2013; respectively S12 and S13 hereafter), Shaw and collaborators obtained optical spectroscopic data for all the FSRQs (S12) and most of the BL Lacs (S13) included in the Second Catalog of AGN Detected by the Fermi LAT (2LAC; Ackermann et al. 2011). We collected from these two papers all the blazars that show broad emission lines in their optical spectra.

In S12, the authors analyzed the optical spectra of 229 FSRQs: they obtained new spectra for 165 FSRQs included in the First Catalog of AGN detected by *Fermi* (1LAC; Abdo et al. 2010), and re–analyzed Sloan Digital Sky Survey (SDSS) spectra of 64 other FSRQs (not all with γ–ray data). Along with spectroscopic data, the authors derived virial black hole masses for all their objects. In order to have a complete description of the sources, we selected only the FSRQs with enough data to fit the entire SED. We are left with 191 objects. We cross–correlated this sample with the 2LAC. When the objects were not included in the 2LAC, we collected data from the 1LAC. The sample was completed including radio data from the Combined Radio All-Sky Targeted Eight GHz Survey (CRATES; Healey et al. 2007). When sources were not included in CRATES (only 5 objects), we obtained radio data at frequencies close to 8 GHz from the ASI Science Data Center (ASDC). We are then left with a sample of 180 FSRQs with optical spectroscopy, along with γ–ray and radio data.

In S13, instead, the BL Lac objects are directly selected from the 2LAC sample. 2LAC includes 475 BL Lacs, among which only 209 have redshift information. We consider here only those objects with broad emission lines, in order to be able to derive an estimate of L_{BLR}, avoiding upper limits. We are left with 26 objects. All of them have 2LAC γ–ray and CRATES radio data. S13 did not derive the black hole masses for these objects. We can anyway assign an average M_{BH} value to these BL Lacs, from an adapted version of the $M_{\mathrm{BH}} - M_R$ relation (from Bettoni et al. 2003), that assumes a mass ratio between bulge and central black hole of 10^3. In fact, BL Lacs are typically hosted in massive and luminous elliptical galaxies, with a small dispersion in absolute magnitude ($\langle M_R \rangle = -22.8 \pm 0.5$; Sbarufatti, Treves & Falomo 2005). Therefore, we can derive an average value of their black hole mass:

$$\log\left(\frac{M_{\mathrm{BH}}}{M_\odot}\right) \simeq -0.5 \times M_R - 3 = 8.4. \qquad (1)$$

Since we need the central black hole masses for our studies, we will apply this value to every object without a mass estimate. These BL Lacs and their relevant data are listed in Table 1.

We add to these new samples the objects that show broad emission lines studied in TS12. Specifically, we add the 45 FSRQs and 1 BL Lac (following our reclassification) that were included in Shen et al. (2011), along with the 15 BL Lacs with broad emission lines from Ghisellini et al. (2011). In this work, we only consider the objects from TS12 that have broad emission lines detected, excluding then all the BL Lacs with only an upper limit on the BLR luminosity. In TS12, the upper limits were introduced to increase the number of BL Lacs, populating the low–luminosity branch of our sample. They followed the $L_{\mathrm{BLR}} - L_\gamma$ correlation already found only with the detections, therefore they were not very constraining. In our new work, we increased the number of BL Lacs with broad emission lines thanks to S13, and therefore we do not need the lineless BL Lacs.

In total, we have 225 FSRQs and 42 BL Lacs with detected

Name [1]	Fermi Name [2]	RA [3]	DEC [4]	z [5]	Line [6]	$\log L_{\rm BLR}$ [7]	$\log L_{\gamma}$ [8]	$\log L_{\rm radio}$ [9]
BL Lac								
GB6 J0013+1910	2FGLJ0013.8+1907	00 13 56.3	+19 10 41.5	0.477	MgII	42.691	45.441	43.043
PKS 0829+046	2FGLJ0831.9+0429	08 31 48.7	+04 29 38.2	0.174	Ha	42.614	45.520	42.923
RBS 0958	2FGLJ1117.2+2013	11 17 06.1	+20 14 07.6	0.138	Ha	41.722	44.723	41.622
PMN J1125-3556	2FGLJ1125.6-3559	11 25 31.3	-35 57 05.0	0.284	Ha	43.338	45.157	42.627
SBS 1200+608	2FGLJ1203.2+6030	12 03 03.4	+60 31 19.1	0.065	Ha	42.005	43.769	41.190
W Comae	2FGLJ1221.4+2814	12 21 31.6	+28 13 58.1	0.103	Ha	42.137	45.055	42.199
PG 1218+304	2FGLJ1221.3+3010	12 21 21.9	+30 10 36.2	0.184	Ha	42.063	45.174	41.734
OQ 530	2FGLJ1420.2+5422	14 19 46.5	+54 23 15.0	0.153	Ha	42.201	44.766	42.603
RGB J1534+372	2FGLJ1535.4+3720	15 34 47.2	+37 15 53.8	0.144	Ha	41.722	44.349	40.991
BL/FS								
PKS 0332-403	2FGLJ0334.2-4008	03 34 13.4	-40 08 26.9	1.357	MgII	45.046	47.711	44.967
TXS 0431-203	2FGLJ0434.1-2014	04 34 07.9	-20 15 17.2	0.928	MgII	43.153	46.511	43.758
PKS 0437-454	2FGLJ0438.8-4521	04 39 00.7	-45 22 23.9	2.017	CIV	45.201	47.661	45.363
PKS 0627-199	2FGLJ0629.3-2001	06 29 23.7	-19 59 19.7	1.724	CIV	44.060	47.740	45.036
4C +14.60	2FGLJ1540.4+1438	15 40 49.5	+14 47 46.5	0.606	MgII	43.575	45.966	44.229
PMN J1754-6423	2FGLJ1755.5-6423	17 54 41.8	-64 23 44.7	1.255	MgII	44.163	46.912	44.113
4C +56.27	2FGLJ1824.0+5650	18 24 07.0	+56 51 01.1	0.664	MgII	43.912	46.891	44.333
S3 2150+17	2FGLJ2152.4+1735	21 52 24.7	+17 34 37.9	0.874	MgII	44.168	46.333	44.310
PMN J2206-0031	2FGLJ2206.6-0029	22 06 43.2	-00 31 02.3	1.053	MgII	43.798	46.557	43.858
B2 2234+28A	2FGLJ2236.4+2828	22 36 22.3	+28 28 58.1	0.79	MgII	44.645	47.079	44.412
PKS 2244-002	2FGLJ2247.2-0002	22 47 30.1	+00 00 07.0	0.949	MgII	44.106	46.543	43.950
PKS 2312-505	2FGLJ2315.7-5014	23 15 44.2	-50 18 39.7	0.811	MgII	43.628	46.357	43.764
PKS 2351-309	2FGLJ2353.5-3034	23 53 47.3	-30 37 48.3	0.737	MgII	43.628	46.066	43.893
FS								
NVSS J020344+304238	2FGLJ0204.0+3045	02 03 44.1	+30 42 38.1	0.761	MgII	44.757	46.449	43.572
PKS 0516-621	2FGLJ0516.8-6207	05 16 44.5	-62 07 04.8	1.3	MgII	44.444	47.488	44.523
MG2 J201534+3710	2FGLJ2015.6+3709	20 15 28.6	+37 10 59.8	0.859	Hb	44.342	47.971	44.794
TXS 2206+650	2FGLJ2206.6+6500	22 08 03.3	+65 19 38.7	1.121	MgII	44.336	47.324	44.360

Table 1. Sources from the S13 BL Lac sample, divided according to their reclassification (see §4). Col. [1]: name; Col. [2]: *Fermi*/LAT counterpart; Col. [3]: right ascension; Col. [4]: declination; Col. [5]: redshift; Col. [6]: line measured, from which $L_{\rm BLR}$ has been derived; Col. [7]: logarithm of the broad line region luminosity (in erg s^{-1}); Col. [8]: logarithm of the γ–ray luminosity from *Fermi* data (in erg s^{-1}); Col. [9]: logarithm of the radio luminosity, calculated at 8 GHz rest–frame (in erg s^{-1}).

broad emission lines, both γ–ray and radio counterparts, and a reliable estimate of the central black hole masses ($M_{\rm BH}$).

2.2 The radio–galaxy sample

We collected a sample of radio–galaxies without broad emission lines from the work by Buttiglione et al. (2010). The authors studied the optical spectroscopical and radio features of all the $z < 0.3$ radio–galaxies (Buttiglione et al. 2009) with $F_{178\rm MHz} > 9$Jy, $\delta > -5^{\circ}$ and an optical counterpart from the Third Cambridge radio catalogue (3CR; Spinrad et al. 1985). The authors classify the sources in high–excitation (HEG), low–excitation galaxies (LEG) and broad line objects (BLO) according to optical features. Specifically, BLOs clearly show broad emission lines, while HEGs and LEGs do not show any broad emission feature, but while the latter have an intrinsic lack of broad line emitting structures, the former show high–excitation fingerprints, suggesting obscuration of the broad line region more than a true absence. The introduction of radio–galaxies in our work aims at studying the true lineless jetted AGN, so we include in our sample the 37 LEGs studied by Buttiglione et al. (2010).

Along with the optical spectral analysis, they performed a radio morphology study. The radio analysis provides information on the core power, which allows us to have a reliable tracer of the inner jet power, without contamination from the extended structures. In other words, the core power traces the same emission that is traced by the radio luminosity in the case of blazars, apart from the different beaming factor (due to the different orientation angles of the jet, see §5). Moreover, the authors provide a measure of the H magnitude, and a calibration to obtain from that the central black hole mass of the objects (Marconi & Hunt 2003):

$$\log\left(\frac{M_{\rm BH}}{M_{\odot}}\right) = -2.77 - 0.464 \times M_H. \qquad (2)$$

The authors find different radio morphologies among the 37 LEGs: 12 FRI, 16 FRII and 9 unclassifiable sources. One object out of each radio group has no M_H information, so we cannot derive a black hole mass estimate. We exclude from our sample those objects.

We are then left with 11 LEGs FRI, 15 LEGs FRII and 8 LEGs without a radio classification (FR?), all with an estimate of the radio core power, with narrow emission line information that give upper limits on the broad emission lines (see §3), and black hole mass estimates. We also added to the radio–galaxy sample M87, a "classic" LEG FRI, taking the radio flux from NED, while the optical spectroscopic information is taken from Buttiglione et al. (2009). M87 does not show any broad emission line, so in the following we will treat it as the LEGs studied by Buttiglione et al. (2010).

3 THE BLR LUMINOSITY

To calculate the BLR luminosity, we need an estimate of the broad emission lines of each object, specifically of Lyα, Hα, Hβ, MgII or CIV. In the case of the S12 FSRQs, we take directly the emission lines fluxes listed in S12, as we did in TS12, while in the case of BL Lacs we directly fit the few broad emission lines present. G11 had already derived from literature the broad emission line values for the BL Lacs included in their sample. Note that the emission lines visible in Mkn421 and Mkn501 spectra have a FWHM ($\sim 1000\,\mathrm{km\,s^{-1}}$) that lies on the classification threshold between narrow lines and broad lines. Therefore, we rather put an upper limit on their broad line luminosities, to be more conservative. We nevertheless leave them in our sample, since they are usually listed as known BL Lacs with lines. The objects included in our radio–galaxy sample have the same issue, being explicitly selected as sources intrinsically lacking broad emission lines. They only show narrow emission lines, so we can obtain from them upper limits on broad emission line luminosities, taking as example quasars with both broad and narrow emission lines. Narrow line–dominated (but with broad emission lines) quasars are in fact included in S11. In their case, the ratio between narrow and broad Hα luminosities is:

$$\frac{L_{\mathrm{nH}\alpha}}{L_{\mathrm{bH}\alpha}} \lesssim 10. \quad (3)$$

In other words, if present, the broad emission lines have a luminosity that is at least 10% the corresponding narrow line luminosity, or more. To be conservative, we choose to fix as a robust upper limit on the broad line luminosity, the luminosity associated to the corresponding detected narrow emission line.

From the broad emission line luminosities or from the upper limits collected for our sample, we can then derive the overall luminosity emitted from the BLR. We follow Celotti et al. (1997) and set the Lyα flux contribution to 100, and the relative weights of the Hα, Hβ, MgII and CIV lines to 77, 22, 34 and 63, respectively (see Francis et al. 1991). The total broad line flux is fixed at 555.76. The L_{BLR} value of each source has been derived using these proportions. When more than one line is present, we calculate the logarithmic average of the L_{BLR} estimated from each line.

3.1 L_{BLR} as a tracer of the accretion

The BLR luminosity is a reliable tracer of the emission from the accretion structure, since the plasma producing the broad emission lines is directly ionized by its radiation. The fraction of disc luminosity that ionizes the plasma in the BLR (photoionizing luminosity, L_{ion}) depends on the geometry of the disc, and hence on its radiation efficiency. In the simplest hypothesis for a radiatively efficient accretion disc (e.g. Shakura & Sunyaev 1973), the disc is geometrically thin and emits as a blackbody at all radii. For simplicity, we approximate the photoionizing luminosity with the entire disc luminosity ($L_{\mathrm{d}} = \eta \dot{M} c^2$). Therefore we can assume that L_{ion} follows the same dependence on the accretion rate as the disc luminosity:

$$L_{\mathrm{ion}} \sim L_{\mathrm{d}} \propto \dot{M}. \quad (4)$$

In this case, then, assuming an average covering factor of $\sim 10\%$ for the BLR, the disc luminosity is $L_{\mathrm{d}} \sim 10 L_{\mathrm{BLR}}$ (e.g. Baldwin & Netzer 1978; Smith et al. 1981). Following the Shakura & Sunyaev hypothesis, such a radiatively efficient disc should occur for $\dot{m} = \dot{M}/\dot{M}_{\mathrm{Edd}} > \dot{m}_c$, where $\dot{M}_{\mathrm{Edd}} = L_{\mathrm{Edd}}/c^2$ and $\dot{m}_c \sim 0.1$ (Narayan & Yi 1995). Sharma et al. (2007) suggested instead that the disc remains radiatively efficient for $\dot{m}_c \gtrsim 10^{-4}$.

	m	q	r
$x = \log L_\gamma$; $y = \log L_{\mathrm{BLR}}$			
(x, y)	0.92±0.19	1.2±14.8	0.81
(x, y), z	0.92±0.19	1.2±14.8	0.59
$x = \log(L_\gamma/L_{\mathrm{Edd}})$; $y = \log(L_{\mathrm{BLR}}/L_{\mathrm{Edd}})$			
(x, y)	0.84±0.20	–2.46±3.1	0.78
(x, y), z	0.84±0.20	–2.46±3.1	0.65
(x, y), z, M	0.84±0.20	–2.46±3.1	0.64

Table 2. Results of the partial correlation analysis of the $L_{\mathrm{BLR}} - L_\gamma$ and $L_{\mathrm{BLR}}/L_{\mathrm{Edd}} - L_\gamma/L_{\mathrm{Edd}}$ relations using a least square fit. The whole blazar sample is taken into account, i.e. 267 objects are considered in the analysis. Correlations are of the form $y = mx + q$. The listed slopes m refer to the bisector (of the two correlations x vs y and y vs x). r is the correlation coefficient obtained from the analysis. We list also the results when accounting for the common dependence on redshift and/or black hole mass. In all the cases, the probability that the correlation is random is $P < 4 \times 10^{-8}$, i.e. all the correlations are statistically relevant.

For values $\dot{m} < \dot{m}_c$ the accretion structure should become radiatively inefficient, switching from a proper accretion disc to a hot accretion flow. In this case, it does not emit as a blackbody, and the overall luminosity decreases and changes its dependence on the accretion rate to $L_{\mathrm{d}} \propto \dot{M}^2$ (Narayan et al. 1997). As a consequence of the change in the emission mode, the ionizing luminosity is no more a relevant fraction of the overall disc luminosity, but $L_{\mathrm{ion}} \ll L_{\mathrm{d}}$. The accretion flow cannot emit as a blackbody, because it is no longer optically thick, and the emission is dominated by synchrotron, bremsstrahlung and comptonization processes (see Yuan & Narayan 2014 for a review). The SED of the accretion flow is therefore very different compared to a Shakura–Sunyaev–like accretion disc (see Fig. 1 in Mahadevan 1997). The photoionizing luminosity (mostly the luminosity emitted in the UV wavelength range) is no more a fixed fraction of the disc luminosity. Since this fraction decreases when the accretion rate decreases, the photoionizing luminosity scales with the accretion rate following a relation steeper than $\propto \dot{M}^2$. Following the model in Mahadevan (1997), in TS12 we estimated the ionizing luminosity for the different accretion rates considered by the author. The UV wavelength range is the most affected from the change in accretion rate of the whole SED, and in fact we found a very steep relation:

$$L_{\mathrm{ion}} \propto \dot{M}^{3.5}. \quad (5)$$

This strong change would lead to an analogous change in the dependence of L_{BLR} on $\dot{M}$.

4 THE L_{BLR}–L_γ RELATION

Figure 1 represents the first result of our work. The left panel shows the BLR luminosity as a function of the γ–ray luminosity. The right panel shows the same quantities divided by the Eddington luminosity (L_{Edd}). The objects included in TS12 are marked as FSRQs or BL Lacs, according to how we classified them in our previous work. The new FSRQs from S12 are included as FSRQs, while the objects classified as BL Lacs in S13 are marked as BL Lacs, BL/FS or FS in the plots. Note that the correlation we found in TS12 is confirmed by the new data, both when directly comparing the two luminosities and when normalizing them by the Eddington luminosity. This clearly strengthens the hypothesis of a tight relation between the

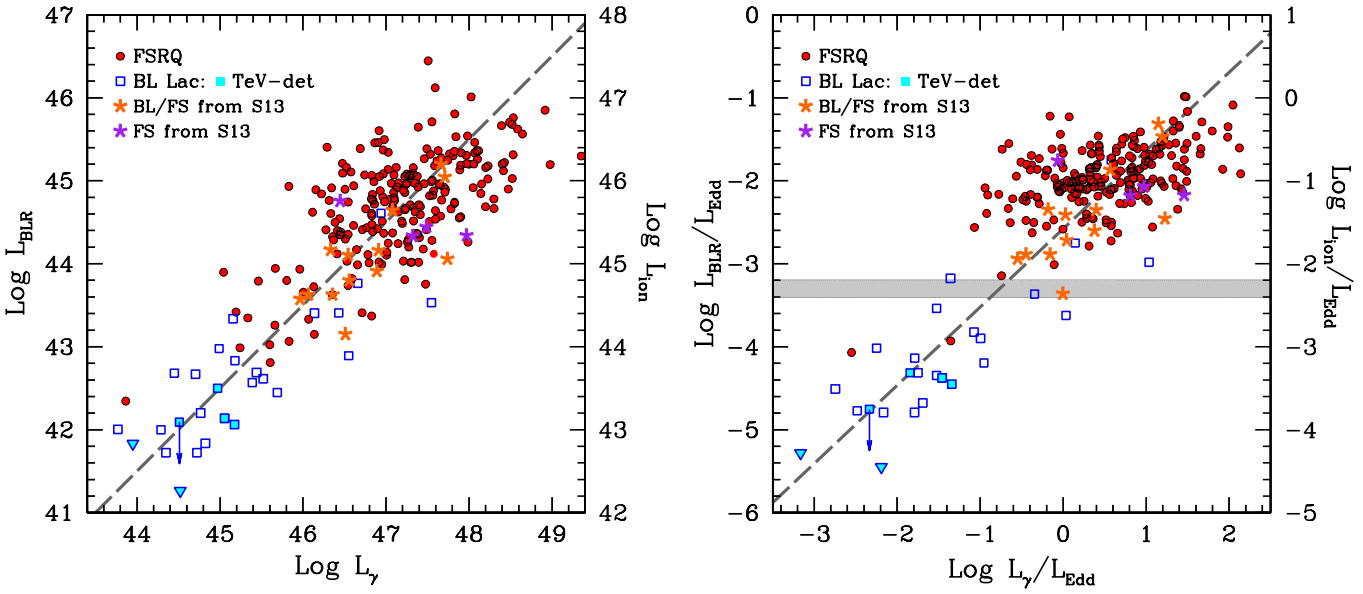

Figure 1. Broad line region luminosity as a function of γ–ray luminosity (left panel) and the same, normalized at the Eddington luminosity (right panel). Different symbols correspond to different classifications, as labelled. The dashed lines are the results of the least square fits described in Table 2. The grey stripe in the right panel indicates the luminosity divide between FSRQs and BL Lacs, located at $L_{\rm BLR}/L_{\rm Edd} \sim 5 \times 10^{-4}$.

accretion rate and the jet power in blazars. As explained in §3.1, the $L_{\rm BLR}$ is a very good tracer of the accretion rate, while the γ–ray luminosity traces well the jet power. We calculate the best fit of the relation between the two luminosities, both normalized by the Eddington luminosity and not. We find that both are consistent with the results found in TS12. We apply a partial correlation analysis, to take also into account the possible common dependence on z and $M_{\rm BH}$ of the values. The $L_{\rm BLR} - L_\gamma$ and $L_{\rm BLR}/L_{\rm Edd} - L_\gamma/L_{\rm Edd}$ relations result linear and statistically relevant (see Table 2).

Contrary to our previous work, instead, the apparent 'divide' between FSRQs and BL Lacs (located at $L_{\rm BLR}/L_{\rm Edd} \sim 5\times10^{-4}$) seems no longer valid, since some BL Lacs from S13 are located in the high–luminosity branch of the correlation, in the area typically occupied by FSRQs (S13 BL Lacs are marked as purple and orange asterisks, or included among the blue empty squares in all the Figures). To understand this discrepancy with our previous results, we first inspected visually the overall SEDs of the BL Lacs from S13. We notice that the sources show three different SED behavior (as shown by the individual SEDs in the Appendix):

- nine have the synchrotron emission dominant or comparable to the high–energy component, and the thermal emission from the accretion structure completely swamped by the non–thermal jet emission. These features define a BL Lac, according to the classification scheme adopted in G11 and TS12, and first introduced by Padovani & Giommi (1995).
- four of them show a clear Compton dominance, and the emission from the accretion disc is clearly visible. We then classify them as FSRQs, and claim for a misclassification in S13. However, we highlight them differently and label them as 'FS', to keep track of them in the plots.
- thirteen objects have the high–energy component that slightly dominates the synchrotron emission, as in the case of non extreme FSRQs. On the other hand, the synchrotron component completely swamps the accretion emission, leading to a BL Lac–like optical appearance. We classify them as 'BL/FS', since they show both a FSRQ and a BL Lac fingerprint.

The objects classified as FS and FS/BL are labelled accordingly in all our Figures. From Figure 1, we immediately notice that all these "reclassified" BL Lacs are the S13 BL Lacs that occupy the high–luminosity branch of our correlations. The FS have all the typical FSRQ features, so we expect to find them in the high–luminosity branch of the $L_{\rm BLR} - L_\gamma$ correlations (see Fig. 1). Interestingly, all the others objects from S13 that were located in the FSRQ branch are the 13 that we classified as BL/FS. Their location allows us to better understand their peculiar SED features. We can in fact infer that they have an intrinsic powerful jet and a highly luminous accretion disc (i.e. high accretion rate), as common FSRQs, even if their optical spectroscopical features are BL Lac–like. In other words, the BL/FS were classified as BL Lacs because of an unusually powerful synchrotron emission that reduced the EW of their broad emission lines, but are instead FSRQs. Even a very luminous thermal continuum, with the related emission features, can in fact be overcome by a very luminous non–thermal continuum (Giommi et al. 2012; 2013). Since the synchrotron emission is mainly driven by the energy density of the magnetic field, we can expect that these objects have it unusually high. This is confirmed by the SED modeling. We fitted the overall SEDs with a one–zone leptonic model (Ghisellini & Tavecchio 2009), and the results show that the energy density of the magnetic field of all the BL/FS is unusually high (detailed results will be shown in Ghisellini et al., in preparation).

Considering the reclassification, the division between FSRQs and BL Lacs at $L_{\rm BLR}/L_{\rm Edd} \sim 5 \times 10^{-4}$ becomes even more relevant. The BL/FS are actually FSRQs "disguised" as BL Lacs and the canonical classification based on the equivalent width of their broad emission lines fails in classifying them. The division based on $L_{\rm BLR}/L_{\rm Edd}$ represents a more physical classifying system, since it discriminates the objects in terms of their accretion rate. However, the divide is not sharp, and again our blazar sample

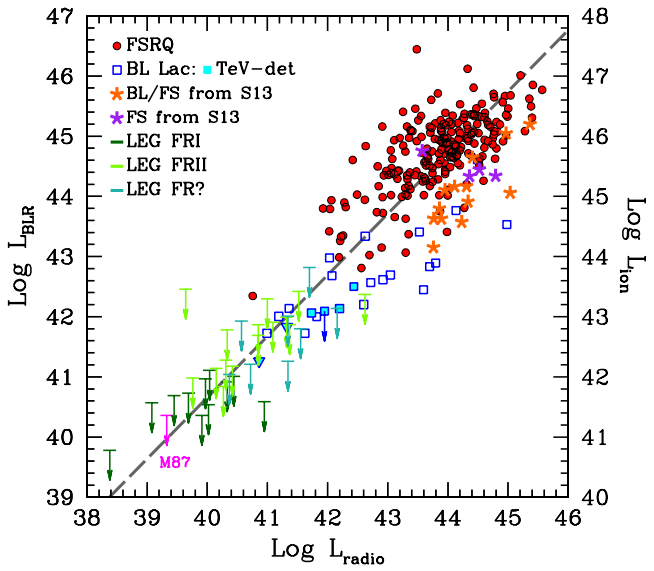

Figure 2. Broad line region luminosity as a function of radio luminosity. Different symbols correspond to different classification of the objects. The dashed line is the result of a least square fit calculated among the detection, i.e. the blazars.

seems to be distributed continuously in both the $L_{\rm BLR} - L_\gamma$ and the $L_{\rm BLR}/L_{\rm Edd} - L_\gamma/L_{\rm Edd}$ planes.

Along with the divide, we are interested in studying at what accretion rate (and if) a change in the accretion structure happens. As detailed in §3.1, a standard Shakura–Sunyaev disc should occur for accretion rates larger than a critical value $\dot{m}_c$. Below that value, the accretion structure is no longer radiatively efficient, also ionizing less efficiently the plasma in the broad line region. This change in accretion should hence be reflected in a change of slope in the $L_{\rm BLR}/L_{\rm Edd} - L_\gamma/L_{\rm Edd}$ plot. The jet power is in fact directly correlated to the accretion rate at all values of the accretion rate itself (Celotti & Ghisellini 2008; Ghisellini et al. 2010). In TS12, the low–luminosity branch of the $L_{\rm BLR}/L_{\rm Edd} - L_\gamma/L_{\rm Edd}$ plot was not populated enough to draw a firm conclusion. The new BL Lacs have increased the number of objects that could help in understanding the possible existence of a break in the relation, but the data are still too sparse to draw a firm conclusion. Hence, we try to have a new perspective on the problem, by introducing another tracer for the jet power, that allows us to reach smaller accretion rates and observe directly the behavior of the jet–disc system in the case of truly inefficient accretion structures, i.e. objects intrinsically without broad emission lines.

5 THE $L_{\rm BLR}$–$L_{\rm RADIO}$ RELATION

We aim to introduce in our study objects that do not have broad emission lines, but with reliable estimates of z and $M_{\rm BH}$, and a direct proxy for the jet power. We also want to be able to derive an upper limit on their BLR luminosity, which we will use as a proxy for $L_{\rm ion}$. As we saw from S13 BL/FS objects, the non–thermal continuum emitted from the jet, highly boosted because of relativistic effects, can dilute dramatically even strong broad emission lines. In the case of less luminous lines, this problem is obviously even bigger. In fact, the majority of γ–ray detected BL Lacs lacks a reliable redshift estimate, since their optical spectra are completely dominated by the non–thermal emission, and they do not show any emission features. This means that we cannot discriminate wether an object is genuinely lineless or its faint emission lines are simply not visible. Hence, to select only truly lineless object, we choose to introduce in our study a sample of radio–galaxies, i.e. jetted AGN in which the optical emission is not completely dominated by the non–thermal, boosted jet emission (sample description in §2.2). We choose a group of LEGs, to be sure that their broad emission lines are not present, likely because of a radiatively inefficient accretion disc. Radio–galaxies are usually not γ–ray detected, so we cannot use the γ–ray luminosity as a tracer of the jet power. We then consider radio luminosity at 8 GHz rest–frame as an alternative jet tracer, with the following caveat: the radio luminosity is emitted from the jet, and is therefore beamed in the emission direction. We will take into account the different beaming factors that characterize blazars and radio–galaxies in the discussion.

Figure 2 shows the comparison between broad line region and radio luminosities in all the sources of our samples. All the radio–galaxies have upper limits on their $L_{\rm BLR}$ values, since they are explicitly selected to be lineless (see §3 for the upper limits derivation). Note that the radio luminosities calculated for blazars and radio–galaxies (and plotted in Figure 2) are differently beamed, because of different viewing angles. Therefore, the linear correlation over the whole luminosity range is only apparent. To properly study the $L_{\rm radio} - L_{\rm BLR}$ relation, we have to homogenize the beaming factors. This is true also if we consider the two luminosities normalized to the Eddington luminosity, as shown in Figure 3, which we analyze in detail in §6.

Note that the objects reclassified as BL/FS are located at the highest radio luminosity edge of the correlation in both Figure 2 and 3. This clearly highlights their FSRQ nature, associated with an uncommonly luminous synchrotron emission, very well traced by the radio luminosity itself. They can easily be considered as the tail at high magnetic field energy density of the class of FSRQs.

Note that in both plots the radio–galaxies are located at $L_{\rm BLR}$ (normalised by $L_{\rm Edd}$ and not) lower than the BL Lacs, with a small overlap. By including these objects, we finally manage to achieve very low disc luminosities, and hence very low accretion rates, which is crucial for our understanding. We discuss the implications of this in §6. The upper limits hint also at a change in relationship between the tracers of $L_{\rm ion}$ and jet power but their presence in the low–luminosity branch of the sample prevents us from a proper parametric characterization of this relation. To understand if the relationship between $L_{\rm BLR}/L_{\rm Edd}$ and $L_{\rm radio}/L_{\rm Edd}$ is better explained by a single or a broken power–law, we do the following: we treat the upper limits as detections and, since these cluster mostly at the low power end, the slope of the power–law we get from the fit has to be considered as a lower limit (i.e., the true value will be steeper). With this approach, we can compare the two hypotheses of a single and a broken power–law by using an F–test. By minimizing the χ^2 values in the hypotheses of a single power–law ($\log L_{\rm BLR}/L_{\rm Edd} = (0.87 \pm 0.12) \log L_{\rm radio}/L_{\rm Edd} + 0.28$) and a broken power–law with break at $L_{\rm radio}/L_{\rm Edd} \sim -4$, we infer that the data are better described by a broken power–law with a 99.97% level of confidence[1]. The break value is fixed to correspond to the dividing value between FSRQs and BL Lacs in $L_{\rm BLR}/L_{\rm Edd}$ discussed in §4, following the single power–law. The broken power–

[1] The uncertainties on $\log L_{\rm BLR}/L_{\rm Edd}$, necessaries to calculate the χ^2, are derived from the uncertainties on the broad line luminosities and on the black hole mass measurements, and are typically $\sim$0.3dex.

law that better fits our data is described by the relation:

$$\log \frac{L_{\rm BLR}}{L_{\rm Edd}} = \begin{cases} (0.98 \pm 0.02) \log \frac{L_{\rm radio}}{L_{\rm Edd}} + 0.72; & \log \frac{L_{\rm radio}}{L_{\rm Edd}} < -4 \\ (0.81 \pm 0.03) \log \frac{L_{\rm radio}}{L_{\rm Edd}} + 0.04; & \log \frac{L_{\rm radio}}{L_{\rm Edd}} \geqslant -4 \end{cases} \quad (6)$$

This shows that a single power law is not a good representation of our data. We discuss in the next section the meaning of this result.

6 DISCUSSION

Figure 3 is the main result of our work. As we have already pointed out, the radio luminosity has a different physical meaning in the case of blazars and radio–galaxies, because of different beaming levels. To properly compare them, we have to beam the radio luminosity of the radio–galaxies, assuming an average bulk Lorentz factor Γ and a viewing angle θ. This will shift them at higher radio luminosities, rejoining them with their aligned analogous AGN. Note that the different orientation of blazars and their parent population does not affect the BLR luminosity, since it is emitted isotropically. Therefore, the parent population of a group of blazars would be located at the same $L_{\rm BLR}/L_{\rm Edd}$, with a $L_{\rm radio}/L_{\rm Edd}$ smaller than the corresponding aligned blazars. From their position in Figures 2 and 3, the LEG FRI radio–galaxies are not the parent population of the BL Lacs included in our study (and see Chiaberge et al. 2000), In fact, it is important to remember that the BL Lacs in our sample have broad emission lines, while the FRI we collected are intrinsically without broad emission lines. This spectral difference explains why our FRI and our BL Lacs are intrinsically different. There is likely a population of *truly lineless BL Lacs* of which these LEGs are actually the parent population, that we are not able to include in our study. The only upper limits on $L_{\rm BLR}$ that we derived for a group of BL Lacs in TS12 (from Plotkin et al. 2011) were anyway located in the same $L_{\rm BLR}$ range as the broad–line BL Lacs. None of the known BL Lacs with a measured redshift represent the re–oriented analogous of the LEG FRI.

However, we are considering only the tip of the iceberg of the BL Lac population: 2LAC includes 475 BL Lacs, and most of them do not have a reliable redshift estimate, since their optical spectra are completely featureless. Without a redshift estimate, we cannot derive their intrinsic luminosity in any band, nor calculate an upper limit on their broad line luminosity. Therefore, they cannot be compared to the other blazars in our work. Among them, there are most likely the truly lineless BL Lacs that would be necessary to study the very low accretion regimes, and of course they would be the aligned analogous to the LEGs that we include in our study. This makes the radio–galaxies without broad emission lines even more relevant for our work, since they are the only valid tracer of the low–accretion regime. But to use them to explore that regime, we have to uniform their beaming to the blazar one.

How much do we have to beam the radio luminosity of the LEGs in our sample to compare them with blazars? The beaming factor of a source with generic Γ, β and θ is:

$$\delta = \frac{1}{\Gamma(1 - \beta \cos\theta)} \quad (7)$$

We take an average viewing angle $\theta_{\rm LEG} \sim 40^\circ$, assuming that the LEGs are misaligned. We want to beam their radio luminosity as they were oriented as a blazar, i.e. with $\theta_{\rm BL} \sim 3^\circ$. Therefore we have to boost the radio luminosity by a factor:

$$\left(\frac{\delta_{\rm BL}}{\delta_{\rm LEG}}\right)^3 = \left(\frac{1 - \beta\cos\theta_{\rm LEG}}{1 - \beta\cos\theta_{\rm BL}}\right)^3 \quad (8)$$

If we assume their jets are beamed with a Lorentz factor similar to a common blazar, i.e. $\Gamma \simeq 10$, this beaming factor would be $\sim 5 \times 10^4$, shifting the LEGs as drawn in Figure 3 (rightmost ellipse). None of the existing blazars could populate that region of the plot, even considering the BL Lacs without redshift. In fact, if we assign an arbitrary $z = 1$ to all BL Lacs without a redshift estimate in 2LAC, we obtain an average radio luminosity at 8 GHz rest–frame $\log L_{\rm radio} \sim 43.2$, that would correspond to $\log(L_{\rm radio}/L_{\rm Edd}) \sim -3.3$. This would not be enough to populate the region occupied by the rightmost ellipse, i.e. the radio–galaxies beamed of a factor $\sim 5 \times 10^4$ due to $\Gamma \simeq 10$. To populate that region, one should postulate the existence of AGN with an extremely powerful and relativistic jet, associated with an accretion structure extremely radiatively inefficient, or even without any accretion structure present. This beaming level seems then quite unlikely.

We can consider another beaming option. From VLBI studies, there is evidence that in strong TeV BL Lacs the pc–scale jets move slowly (Edwards & Piner 2002; Piner & Edwards 2004). At the same time, the extreme variability of their intense TeV luminosity implies that the jet should be highly relativistic, at least in the region where the TeV emission originates. To justify such a discrepancy, the two less demanding hypothesis that have been advanced are: (i) a deceleration of the emitting region between the TeV and the radio locii (Georganopoulos & Kazanas 2004); and (ii) a spine–layer structure of the jet (Ghisellini et al. 2005). Furthermore, detailed observations performed with the VLBI show a morphology that suggests the presence of a slower external layer, surrounding a faster core in the jet in the lineless BL Lac Mkn 501 (Giroletti et al. 2004). Similar results have also been obtained in the case of some radio–galaxies (Giovannini et al. 1999; Swain et al. 1998; Owen et al. 1989). Moreover, a velocity structure helps in explaining other features typical of radio–galaxies, such as the configuration of their magnetic field (Komissarov 1990; Laing 1993). According to this hypothesis, the radio emission should then be characterized by a rather small Lorentz factor $\Gamma \sim 3$, being emitted by the external layer. In this case, the LEG radio luminosity can be boosted by a smaller factor $(\delta_{\rm BL}/\delta_{\rm LEG})^3 \sim 100$.

The central ellipse in Figure 3 represents this hypothesis. Such a beaming factor shifts the radio power of the LEGs by such an amount that in the $L_{\rm BLR}/L_{\rm Edd} - L_{\rm radio}/L_{\rm Edd}$ plane they now follow a much steeper relationship than the almost linear best fit derived in §5 with the broken power–law. As previously done, we perform an F–test to compare the single and a broken power–law hypotheses, obtained as best fits of our data, all assumed as detections. The two best fits are $\log L_{\rm BLR}/L_{\rm Edd} = (0.89 \pm 0.19) \log L_{\rm radio}/L_{\rm Edd} + 0.36$ and again a broken power–law with break at $L_{\rm radio}/L_{\rm Edd} \sim -4$:

$$\log \frac{L_{\rm BLR}}{L_{\rm Edd}} = \begin{cases} (2.00 \pm 0.06) \log \frac{L_{\rm radio}}{L_{\rm Edd}} + 4.8; & \log \frac{L_{\rm radio}}{L_{\rm Edd}} < -4 \\ (0.78 \pm 0.03) \log \frac{L_{\rm radio}}{L_{\rm Edd}} - 0.08; & \log \frac{L_{\rm radio}}{L_{\rm Edd}} \geqslant -4 \end{cases} \quad (9)$$

The F–test shows that, again, a broken power–law provides a better description of the data at the $> 99.99\%$ level. We stress again that the slope derived with this method at values below the break provides *only a lower limit* to the true slope. In other words, at luminosities smaller than the break, jetted AGN follow a relation steeper than:

$$\frac{L_{\rm BLR}}{L_{\rm Edd}} \propto \left(\frac{L_{\rm radio}}{L_{\rm Edd}}\right)^2 \quad (10)$$

This clearly means that the jetted AGN highlight the break

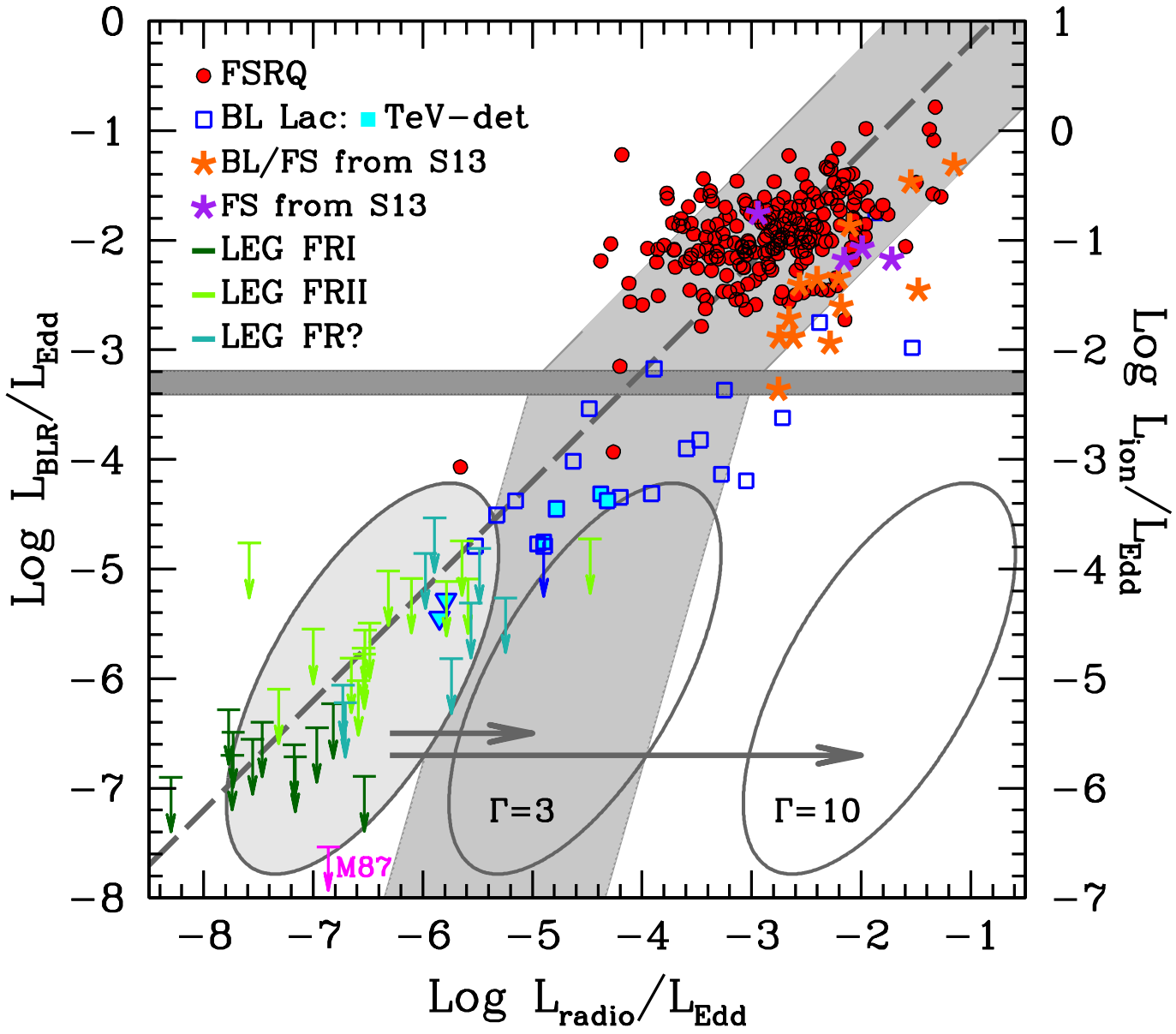

Figure 3. Luminosity of the broad line region (in Eddington units) for the sources from our samples as a function of the radio luminosity (in Eddington units). Different symbols correspond to different samples or a different classification of the sources, as labelled. The dashed lines indicate the bisector, rescaled to pass through the FSRQs. The dark grey horizontal stripe indicates the luminosity divide between FSRQs and BL Lacs at $L_{\rm BLR}/L_{\rm Edd} \sim 5\times10^{-4}$. The light grey stripe indicates the expected distribution of the luminosities if they were produced by a Shakura–Sunyaev accretion disc for $L_{\rm BLR}/L_{\rm Edd} \sim 5\times10^{-4}$ and an ADAF with a Mahadevan–like spectrum ($L_{\rm d} \propto \dot{m}^{3.5}$, see §3.1 and §6). The leftmost ellipse include the core of the radio–galaxies of our sample. The central and rightmost ellipses show where the radio–galaxies would be located if they were beamed according to Lorentz factors $\Gamma = 3$ or 10, respectively (as indicated by the arrows, and described in §6).

that we expect from standard theory of accretion discs, i.e. there is a change in the accretion process at $L_{\rm BLR}/L_{\rm Edd} \approx 10^{-3.5}$ (the light grey stripe in Figure 3). In fact, if we interpret the LEGs as the jetted AGN with lowest accretion rate, as suggested by their $L_{\rm BLR}$, they would follow a relation that is steeper than the one expected in the case of an efficient accretion structure (i.e. linear). This relation is even steeper than the simple dependence of $L_{\rm d}$ on the accretion rate ($L_{\rm d} \propto \dot{M}^2$), since the slope we derive is only a lower limit on the true slope. This result is consistent with highly radiatively inefficient models, closer to the most inefficient one, i.e. a pure ADAF, from which we expect the relation

$$\frac{L_{\rm BLR}}{L_{\rm Edd}} \propto \frac{L_{\rm ion}}{L_{\rm Edd}} \propto \dot{m}^{3.5}. \qquad (11)$$

below the value of $\dot{m}_c$, which separates the two accretion regimes.

We find that such a transition occurs at $\dot{m}_c \sim 0.1$, i.e. $L_{\rm BLR}/L_{\rm Edd} \sim 5\times10^{-4} - 10^{-3}$ if a radiative efficiency $\eta \sim 0.1$ is assumed. This threshold is consistent also with the accretion rate transition between FRI and FRII found by Ghisellini & Celotti

(2001). The hypothesis of a transition at $\dot{m}_c \sim 10^{-4}$ would not be consistent with the beamed LEG data. In any case, we do not expect a sharp transition, but more likely a smooth one, since we do not observe a clear bimodality in the $L_{\rm BLR}/L_{\rm Edd}$ distribution.

7 CONCLUSIONS

In this work, we have explored the connection between jet and accretion structure in jetted AGN, using 267 broad emission line blazars and 38 broad–line–less radio–galaxies, all with known redshift, a measure of the jet power and an estimate of the black hole mass. In the case of blazars, we have used both γ–ray and radio luminosities to trace their jet power, while the radio–galaxies only have the radio core power as a jet tracer. Since they do not show broad emission lines, we have derived robust upper limits on their broad line region luminosity from the luminosity of their narrow lines. They are crucial to explore the low–accretion regime of jetted AGN. The results we obtained can be summarized as follows:

(i) With a sample composed by both blazars and radio–galaxies, we finally can identify the transition between efficient and inefficient accretion structures. With only blazars, we are not able to include the very low–accreting objects, since they would be lineless and dominated by the jet non–thermal emission, and therefore again without a redshift estimate. LEG radio–galaxies are therefore the only mean to study the radiatively inefficient accretion regime.

(ii) The most reasonable beaming option for the radio–galaxies we included is due to jets structured with a central extremely relativistic spine, surrounded by a slower layer. A high Lorentz factor $\Gamma = 10$, necessary to justify some observational properties, would characterize only the central part of the jet. A slower layer likely surrounds this extreme spine, and would be the responsible of the radio emission from the jet. This external layer is characterized by a smaller Lorentz factor ($\Gamma \sim 3$), implying a smaller beaming factor to homogenize radio–galaxies to blazars.

(iii) The transition between efficient and inefficient accretion regimes occurs at the standard critical value $\dot{m}_c \sim 0.1$, i.e. at $L_{\rm BLR}/L_{\rm Edd} \sim 5 \times 10^{-4} - 10^{-3}$ assuming an accretion efficiency $\eta \sim 0.1$. At accretion values lower than that, the ionizing luminosity decreases with a slope steeper than $\propto \dot{m}^2$, clearly traced by the radio–galaxies. This is consistent with a transition from an efficient to an inefficient regime at low accretion rates. A relevant decrease in the ionizing luminosity is in fact expected in all the highly inefficient accretion regimes (e.g. the ADAF model).

ACKNOWLEDGMENTS

We thank the referee for useful comments that improved the paper. Part of this work is based on archival data, software or online services provided by the ASI Data Center (ASDC). This research made also use of the NASA/IPAC Extragalactic Database (NED) which is operated by the Jet Propulsion Laboratory, Caltech, under contract with NASA.

REFERENCES

Abdo A.A., Ackermann M., Ajello M. et al., 2010, ApJ, 715, 429
Ackermann M., Ajello M., Allafort A., et al., 2011, ApJ, 743, 171
Baldwin J.A & Netzer H., 1978, ApJ, 226, 1
Baum S.A., & Heckman, T., 1989a, ApJ, 336, 681
Baum, S.A., & Heckman, T., 1989b, ApJ, 336, 702
Bettoni D., Falomo R., Fasano G., Govoni F., 2003, A&A, 399, 869
Buttiglione S., Capetti A., Celotti A., et al., 2009, A&A, 495, 1033
Buttiglione S., Capetti A., Celotti A., et al., 2010, A&A, 509, 6
Capetti A., Raiteri C.M., Buttiglione S., 2010, A&A, 349, 77
Celotti A., Padovani P., & Ghisellini G., 1997, MNRAS, 286, 415
Celotti A. & Ghisellini G., 2008, MNRAS, 385, 283
Edwards P.G. & Piner B.G., 2002, ApJ, 579, 67
Fanaroff B.L., Riley J.M, 1974, MNRAS, 167, 31
Francis P.J., Hewett P.C., Foltz C.B., Chaffee F.H., Weymann R.J. & Morris S.L., 1991, ApJ, 373, 465
Georganopoulos M. & Kazanas D., 2004, ApJ, 604, 81
Ghisellini G. & Celotti A., 2001, A&A, 379, L1
Ghisellini G. & Tavecchio F., 2009, MNRAS, 397, 985
Ghisellini G., Tavecchio F. & Chiaberge M., 2005, A&A, 432, 401
Ghisellini G., Tavecchio F., Foschini L., Ghirlanda G., Maraschi L. & Celotti A., 2010, MNRAS, 402, 497
Ghisellini G., Tavecchio F., Foschini L, Ghirlanda G., 2011, MNRAS, in press (G11)
Giommi P., Padovani P., Polenta G., Turriziani S., D'Elia V., Piranomonte S., 2012, MNRAS, 420, 2899
Giommi P., Padovani P., Polenta G., 2013, MNRAS, 431, 1914
Giovannini G., et al., 1999, ApJ, 522, 101
Giroletti M., Giovannini G., Feretti L., et al., 2004, ApJ, 600, 127
Healey S.E., et al. 2007, ApJS, 171, 61
Komissarov S.S., 1990, SvA, 16, L284
Labiano A., 2008, A&A, 488, L59
Landt H., Padovani P., Giommi P. Perlman E.S., 2004, MNRAS, 351, 83
Laing R., 1993, in Burgarella D., Livio M., ODea C., eds, Astrophysical Jets. Cambridge Univ. Press, Cambridge, p. 95
Laing R.A., Jenkins C.R., Wall J.V., & Unger S.W., 1994, in The Physics of Active Galaxies, ed. G. V. Bicknell, M.A. Dopita, & P.J. Quinn, ASP Conf. Ser., 54, 201
Mahadevan R., 1997, ApJ, 447, 585
Marconi A. & Hunt L.K. 2003, ApJ, 589, L21
Morganti R., Tadhunter C.N., Dickson R., & Shaw M., 1997, A&A, 326, 130
Narayan R., Garcia M.R. & McClintock J.E., 1997, ApJ, 478, L79
Narayan R. & Yi I., 1995, ApJ, 452, 710
Owen F.N., Hardee P.E. & Cornwell T.J., 1989, ApJ, 340, 698
Padovani P. & Giommi P., 1995, ApJ, 444, 567
Piner B.G. & Edwards P.G., 2004, 600, 115
Plotkin R.M., Markoff S., Trager S.C. & Anderson S.F., 2011, MNRAS, 413, 805
Rawlings S., & Saunders R., 1991, Nature, 349, 138
Rawlings S., Saunders R., Eales S.A., & Mackay C.D., 1989, MNRAS, 240, 701
Sbarrato T., Ghisellini G., Maraschi L., Colpi M., 2012, MNRAS, 421, 1764 (TS12)
Sbarufatti B., Treves A. & Falomo R., 2005, ApJ, 635, 173
Shakura N.I. & Sunyaev R.A., 1973 A&A, 24, 337
Sharma P., Quataert E., Hammet G.H. & Stone J.M., 2007, ApJ, 667, 714
Shaw M.S., et al., 2012, ApJ, 748, 49 (S12)
Shaw M.S., et al., 2013, ApJ, 764, 135 (S13)
Shen Y., Richards G.T., Strauss M.A. et al., 2011, ApJS, 194, 45
Smith M.G., Carswell R.F., Whelan J.A.J. et al., 1981, MNRAS 195, 437
Spinrad H., Marr J., Aguilar L. & Djorgovski S. 1985, PASP, 97, 932
Swain M.R., Bridle A.H., Baum S.A., 1998, ApJ, 507, 29
Urry C.M. & Padovani P., 1995, PASP, 107, 803
Vermeulen R.C., et al., 2005, ApJ, 452, L5
Willott C.J., Rawlings S., Blundell K.M., & Lacy M., 1999, MNRAS, 309,1017

APPENDIX

We show in Figures 4, 5 and 6 the SEDs of the 25 objects from S13, divided according to our reclassification, discussed in §4. The

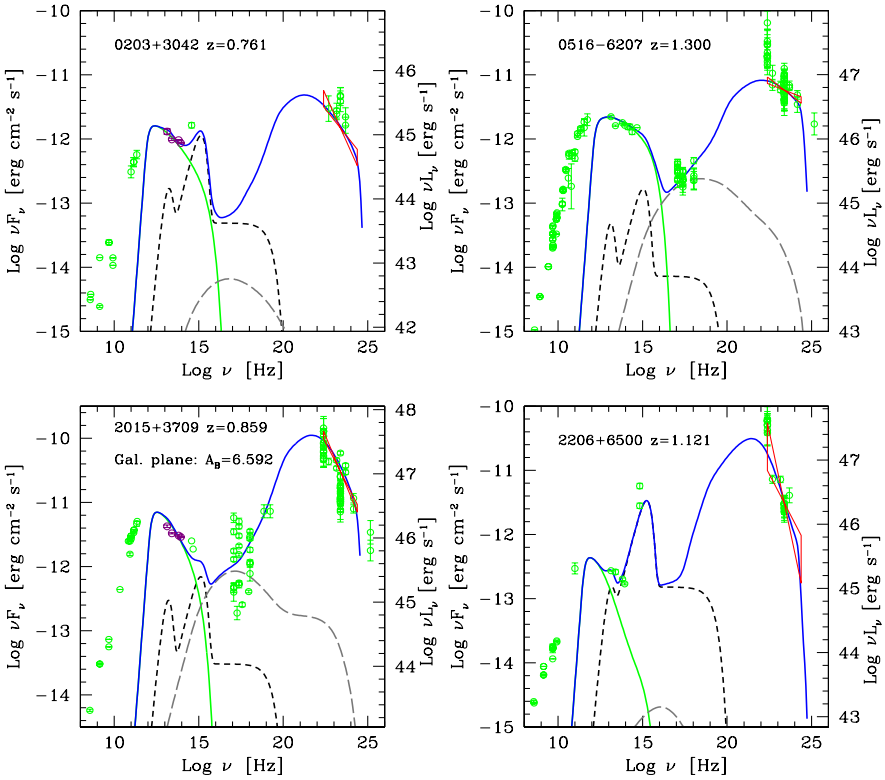

Figure 4. Sources reclassified as FS. The blue solid lines represent the overall models. The green solid line is the synchrotron components, the black dashed line is the thermal emission from accretion disc, torus and corona, while the grey long–dashed line is the Synchrotron–Self–Compton emission.

SEDs are fitted with a one–zone leptonic model, fully described in Ghisellini & Tavecchio (2009).

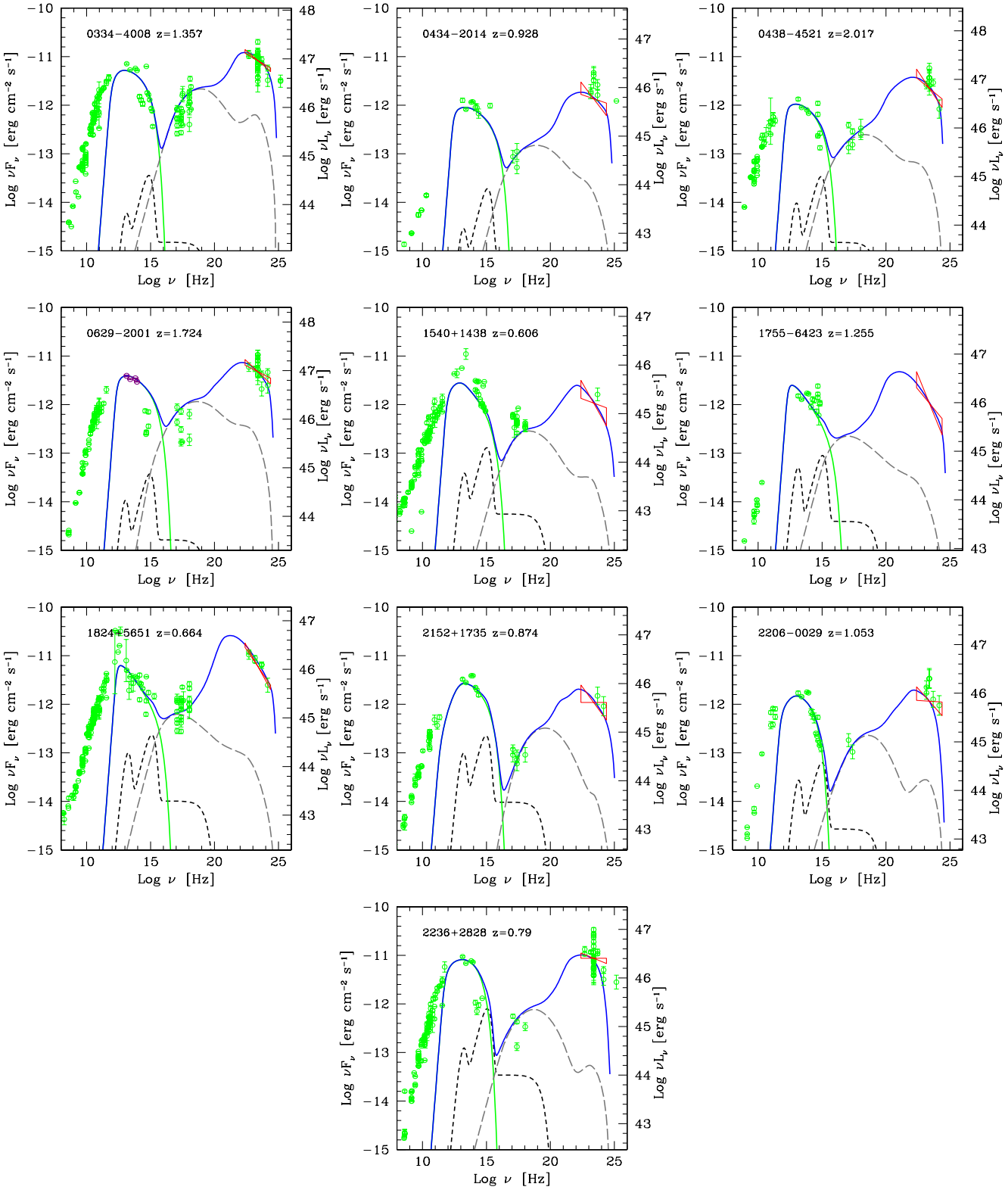

Figure 5. Sources reclassified as BL/FS, with optical spectra showing weak broad emission lines, but SEDs more typical of FSRQs. Lines as in Figure 4.

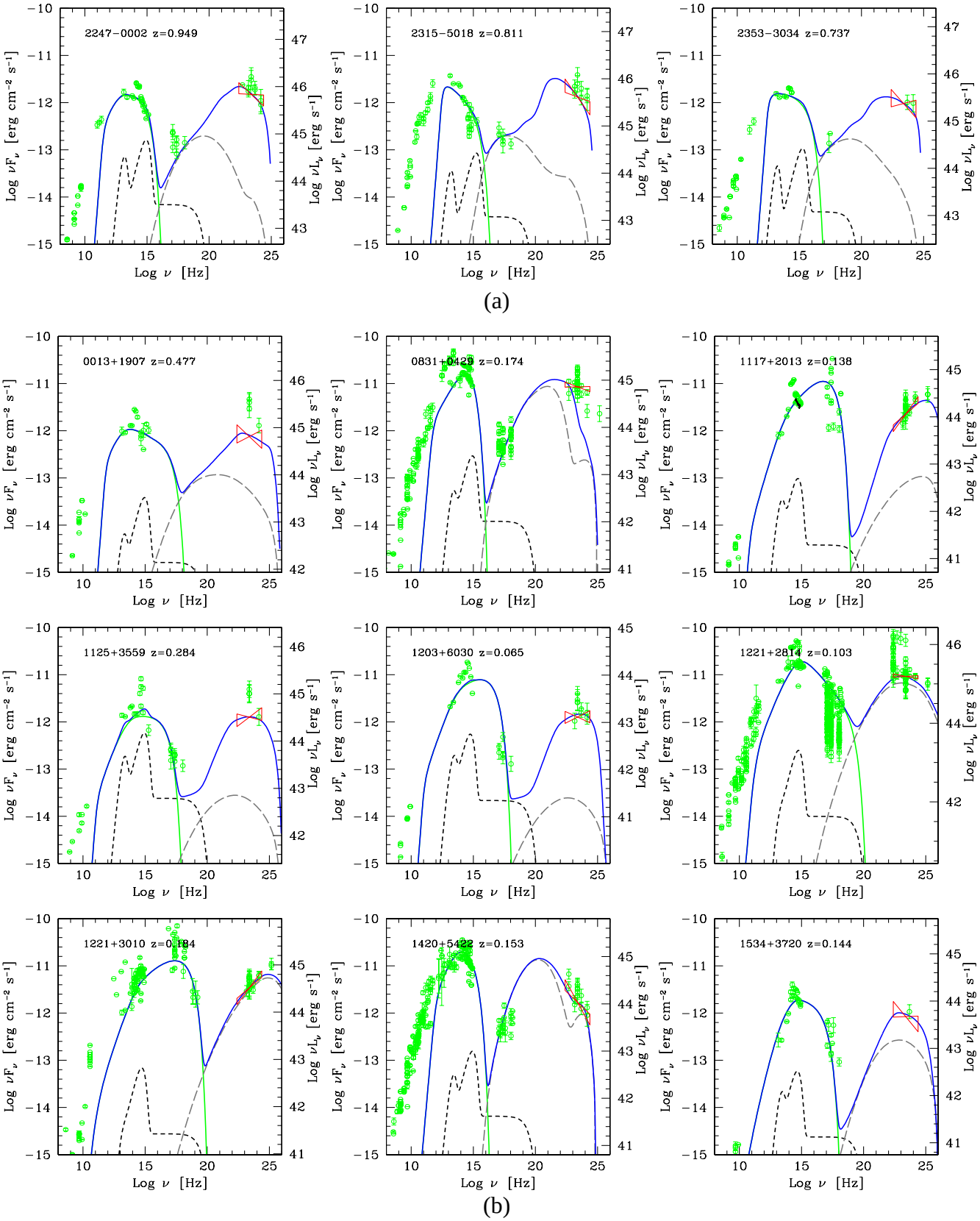

Figure 6. (a) Sources reclassified as BL/FS. (b) Sources that can be classified as BL Lacs, both from the optical spectra and from the SED aspect. Lines as in Figure 4.